Research article

A novel PVDF microforce/force rate sensor for practical applications in micromanipulation

Yantao Shen
Ning Xi
King W.C. Lai and
Wen J. Li

The authors

Yantao Shen and **Ning Xi** are based at the Michigan State University, East Lansing, Michigan, USA.
King W.C. Lai and **Wen J. Li** are based at The Chinese University of Hong Kong, Hong Kong SAR, People's Republic of China.

Keywords

Microsensors, Assembly, Force

Abstract

This paper presents our development of a novel force and force rate sensory system to advance applications in micromanipulation using an *in situ* polyvinylidene fluoride (PVDF) piezoelectric sensor. To allow close monitoring of magnitude and direction of microforces acting on microdevices during manipulation, PVDF ploymer films are used to fabricate highly sensitive 1D and 2D sensors to detect real-time microforce and force rate information during the manipulation process. The sensory system with a resolution in the range of sub-micronewtons can be applied effectively to develop a technology on the force-reflection microassembly of surface MEMS structures. In addition, a tele-micromanipulation platform, which can be used to perform tele-microassembly of the MEMS structures and tele-cell-manipulation with force/haptic feedback via Internet was also built successfully.

Electronic access

The Emerald Research Register for this journal is available at
www.emeraldinsight.com/researchregister

The current issue and full text archive of this journal is available at
www.emeraldinsight.com/0260-2288.htm

1. Introduction

Microfabrication methods such as bulk-micromachining and surface-micromachining are commonly used to make devices for a wide variety of applications, including sensing, optical and wireless communications, digital display, and biotechnology. Despite the enormous research in creating new applications with MEMS, the research efforts at the backend, such as automatic microassembly and packaging, are relatively limited. One main reason for such limitation is that the manipulation of microsized objects is poorly understood (Nelson *et al.*, 1998). Owing to scaling effects, unmodeled forces that are insignificant at the macroscale become dominant at the microscale (Fearing, 1995). For example, when the part is less than 1 mm in size, adhesive forces between the manipulator and the part can be significant compared to gravitational forces. These adhesive forces arise primarily from surface tension, van der Waals, and electrostatic attractions and the measurement of those forces will be a critical factor for micropart manipulation. As a case in point, manufacturing processes which are capable of efficiently assembling MEMS devices such a micromirror in optical switches have not been developed, partially because, at the microscale, structures are fragile and easily breakable. They typically break at the micronewton force range that cannot be reliably measured by existing force sensors (Fatikow *et al.*, 2000). The micromirror components are usually surface optomechanical structures. They lie on the surface of substrate after fabrication processes, as shown in Figure 1(a). An assembly process is needed to rotate it up to a perpendicular position as shown in Figure 1(b) and (c). The most straightforward and flexible method is to use microprobes to physically manipulate the mirror into the position. However, this process can be inherently risky without knowledge of the force(s) being applied and slow without some level of precision and automation. It has been widely realized that there have not been a reliable sensor for accurately obtaining microforce data during assembly, and force/impact control method for effectively regulating the contact force/impact in the micromanipulation (Böhringer *et al.*, 1999; Cohn *et al.*, 1998; Kenny, 2001). As a result, the microdevices are often damaged during assembly, which decrease overall yield and drives up cost significantly. It has been estimated that assembly

This work is supported in part by the NSF Grants IIS-9796300, IIS-9796287, EIA-9911077, Hong Kong Research Grants Council (CUHK4206/00E), and by the Chinese Academy of Sciences' Distinguished Overseas Scholar Grant.

Sensor Review
Volume 24 · Number 3 · 2004 · pp. 274–283
 · ISSN 0260-2288
DOI 10.1108/02602280410545407

Figure 1 (a) Micromirrors on the chip; (b) a force is applied at the mirror; (c) the automatic latches lock the mirror in upright position

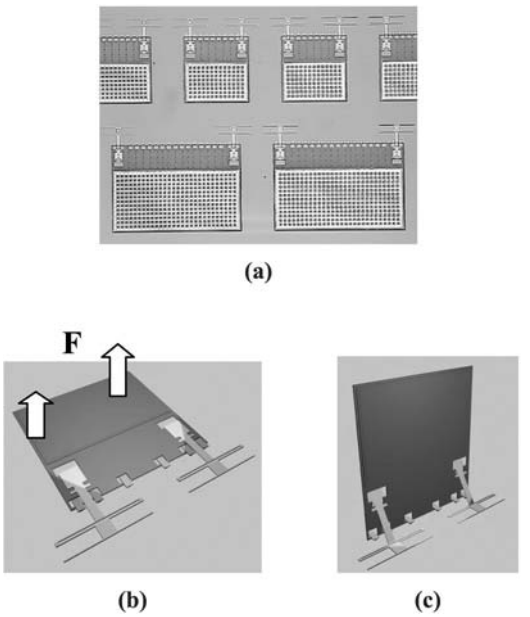

cost of microdevices can run as high as 80 percent of the total production cost (Koelemijer *et al.*, 1999).

Besides microassembly, recent advances in microbiology such as cloning demonstrate that increasingly complex micromanipulation strategies for manipulating biological cells are required (Sun and Nelson, 2001; Sun *et al.*, 2001). For example, cell manipulation or injection is one of the important tasks in microbiology, as shown in Figure 2. Conventionally, cell manipulation is conducted manually. Operators often require at least 1 year full time training to become proficient at the task, even so, the operators still need to spend sufficient time on a manipulation task, and success rate is disappointingly low (about 2 percent). The reason for this is that successful manipulation is determined greatly by speed, trajectory and manipulating forces (Kimura and Yamagimachi, 1995). As a result, this situation calls for the automatic microbiology technique: bio-manipulation, which can entail precise operations such as positioning, grasping, and injecting material into various locations in cells other than cell injury. Typically, the existing microbiomanipulation techniques can be classified as non-contact manipulation including laser trapping and electro-rotation, and contact manipulation referred to mechanical micromanipulation. For non-contact methods, the damage caused by laser beams in the laser trapping technique and the lack of a holding cell mechanism in the electro-rotation technique always make the limits on application of non-contact microbiomanipulation. Although the existing mechanical biomanipulations overcome the drawbacks of non-contact methods, however it can only achieve high accuracy in cell position, the successful rate of microbiomanipulation can still not be improved without the effective microforce sensing and control during cell manipulations.

Figure 2 Cell manipulation of fruit fly embryo

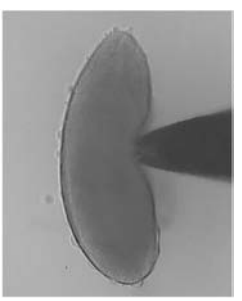

Currently, reference to various sensing mechanisms and control schemes developed (Arai *et al.*, 1996; Carrozza *et al.*, 2000; Nelson *et al.*, 1998; Zesch and Fearing, 1998), it is evident that no single microassembly and biomanipulation technology stands out as being the most promising method since the lack of effective methods on microforce sensing and control. Fortunately, upon the summary of the applications of piezoelectric sensing and control (Lee *et al.*, 1996; Yamagata and Higuchi, 1995), it can be found that the piezoelectric effect material such as polyvinylidene fluoride (PVDF) is highly sensitive to deflection from which force data can be extracted (Benech *et al.*, 1996; Fung *et al.*, 2002; Measurement Specialities Inc., 1999; Roh *et al.*, 2002). And it is one of the most suitable materials to design a high sensitivity force sensor for micromanipulation.

The objective of this paper is to develop a feasible and versatile solution in microassembly and biomanipulation, i.e. designing a highly sensitive PVDF force sensor to measure contact/impact force and its rate so as to enable a regulation of force/impact during the microassembly process and biomanipulation. By integrating the PVDF sensor on a probe-tip used for contact micromanipulation and assembly, the microcontact force signal and its rate can be extracted and processed by a custom-built electronic circuit, and the integrated sensor can be used to efficiently regulate the contact/impact force, and thus keep a safety margin during assembly and biomanipulation. Its applications could be an important step to make reliable and high yield batch fabrication, assembly of MEMS and highly efficient microbiology a reality.

Sensor Review
Volume 24 · Number 3 · 2004 · 274–283

2. Sensor modeling and design

2.1 PVDF microforce/force rate sensors

For the 1D sensor model (Figure 3), the relationship between the output voltage $V(t)$ and the microcontact force rate $\dot{F}(t)$ can be found as

$$V(t) + \lambda \dot{V}(t) = B\dot{F}(t) \tag{1}$$

where

$$\lambda = R_P C_P \text{ and } B = \frac{R_P W L d_{31} h\left(L_0 + \frac{L}{2}\right)}{2I}$$

are constants. R_P, C_P are the resistance and capacitance of the PVDF film, respectively. d_{31} is the transverse piezoelectric coefficient. I represents the inertial moment of cross-sectional area a.

Based on the 1D model, as shown in Figure 4, the 2D sensor was designed using a parallel beam structure. In each direction, a two-piece parallel beam is used to improve the rigidity of the structure and, at the same time, to keep the sensitivity of the force sensing in that direction. It can also be seen that this structure provides a decoupling force measurement in the *Y*- and *Z*-directions.

The decoupled output voltages and force rates can be represented as

$$\begin{aligned} V_Z(t) + \lambda_Z \dot{V}_Z(t) &= B_Z \dot{F}_Z(t) \\ V_Y(t) + \lambda_Y \dot{V}_Y(t) &= B_Y \dot{F}_Y(t) \end{aligned} \tag{2}$$

Furthermore, the proposed PVDF force sensor can also be extended to 3D force sensing, as shown in Figure 5. Based on the design of the 2D sensor, another slab of the PVDF film can be placed at the front cross-section to provide the force measurement in the *X*-direction.

Figure 3 Illustration of 1D sensor structure

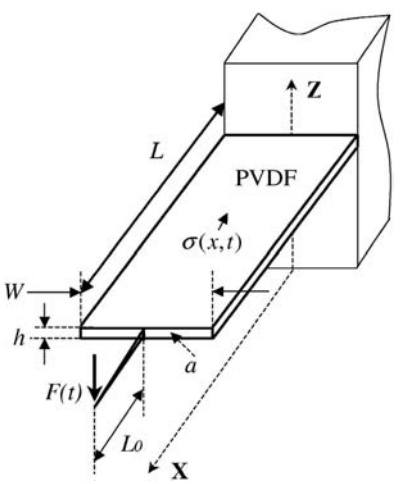

Figure 4 Illustration of 2D sensor structure

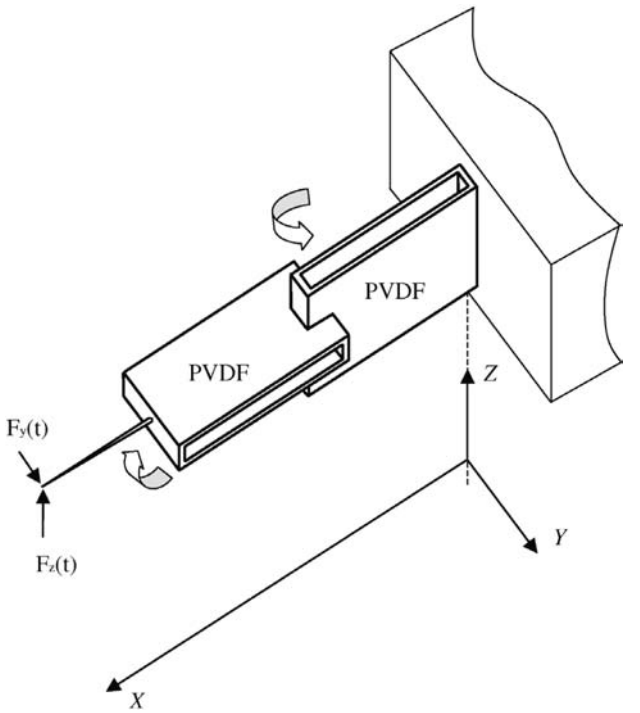

2.2 Signal conditioning circuit

Preprocessing of sensed data by the circuit is critical for three reasons:

(1) to remove noises (from vibrations, temperature change, external electronic coupling noises etc.);
(2) to amplify and extract the desired signal which is in this case the force and force rate; and
(3) to expand the low frequency response of the PVDF sensors. The simplified diagram of developed circuit is shown in Figure 6.

In this circuit, a differential charge amplifier was designed for the PVDF force sensor. The differential charge amplifier is based on the chopper stabilized operational amplifier TC7650C with a high input impedance $10^{12}\,\Omega$ and low bias current 1.5 pA.

A high input impedance can avoid bleed-off of the charge on the feedback capacitor C_{f1} and C_{f2}, and low bias current prevents the feedback capacitor from charging and discharging at excessive rates. Following the charge amplifier, a differential-to-single-ended amplifier is added. In this design, the total differential topology can reduce the common mode noises more effectively. Otherwise, by choosing the charge amplifier, the cable capacitor C_c is removed from the dynamic model of the circuit, so that a long cable can be used to connect the sensor and circuit without affecting the system sensitivity. With the use of the charge amplifier, the sensor can measure force at

Figure 5 Illustration of 3D sensor structure

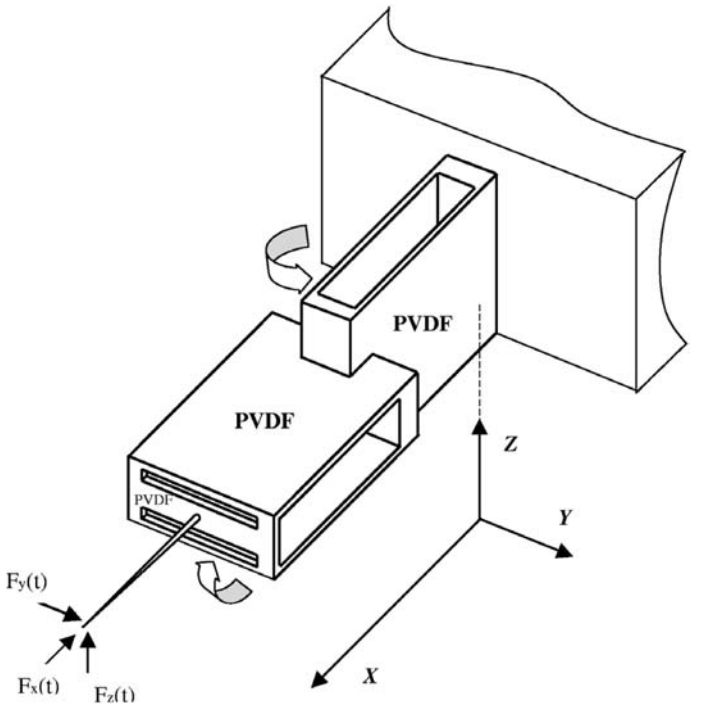

a very low frequency, this is because the low corner frequency is now expanded to

$$f_l = \frac{1}{2\pi R_{fi} C_{fi}},$$

where i is the index for 1 or 2.

As shown in the diagram of the circuit, resistors R_{c1} and R_{c2} can provide electrostatic discharge (ESD) protection.

Owing to the vibration, thermal noises are the major high frequency disturbances of sensor signal. To reject the high frequency noises, an active low pass filter with the suitable cut-off frequency was used before the voltage output. An integrator unit in the circuit can also achieve the integration of the output voltage/time. In addition, cable motion (triboelectric effect) was removed by using a shielded cable with low capacitance. The reduction of both radio frequency interference (RFI) and electromagnetic interference (EMI) was handled by the related filtering and shielding in the circuit. Moreover, the operational amplifier casing was well grounded and the sensor inputs were guarded and connected to the same ground as the casing.

The complete processing circuit can be integrated on a single microelectronic chip, which can measure the differential voltage across the sensor and provides a filtered version of the force rate and the force. The integrated electronic circuit can achieve the following:

(1) low noise processing amplification using low-noise electronic elements designed at the transistor level;
(2) high-frequency noise-filtering via low pass filtering;
(3) sensor dynamic model compensation; and
(4) principal component analysis (PCA) computation to detect the presence and direction of force. This last stage may instead be post computed in software.

By considering the sensor model and whole circuit, then global transfer function of the sensor system is

$$\frac{V_{\text{out}}(s)}{F(s)} = \frac{V_{\text{c}}(s)\text{BK}_{\text{c}}}{\lambda} \frac{\lambda s}{(1+\lambda s)(1+\tau_1 s)} \qquad (3)$$

The function is a bandpass type filter. K_{c} is the gain of the differential-to-single-ended amplifier.

Figure 6 Schematic of the developed electronic circuit

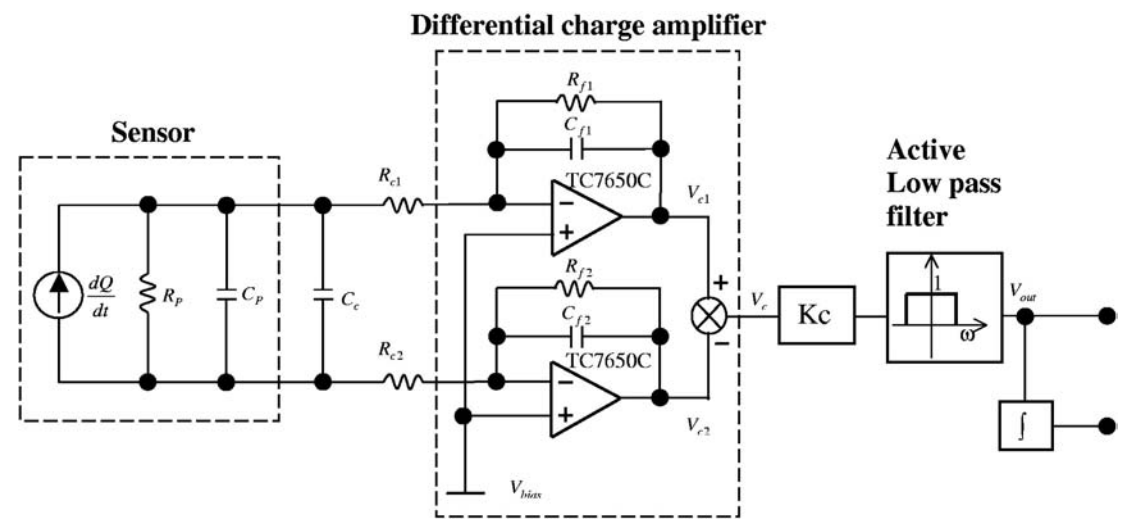

τ_1 is small time constant of the active low pass filter. By filtering this signal over an appropriate passband and then integrating with respect to time, that generates the force rate and the force, over this passband, respectively.

3. Sensor calibration

3.1 Experimental set-up

Referring to the basic physical models of the 1D and 2D PVDF sensors, Figure 7 shows the prototypes of the PVDF sensors used in the calibration and experiments. As shown in figure, the PVDF force sensor (1D) has the following dimensions and parameters:

$$L_0 = 0.0225\,\text{m},\quad L = 0.0192\,\text{m},\quad W = 0.0102\,\text{m},$$

$$h = 28\,\mu\text{m}\ \ (\text{PVDF film}),\quad R_P = 1.93\times10^{12}\,\Omega,$$

$$C_P = 0.90\times10^{-9}\,\text{F},\quad E = 2\times10^{-9}\,\text{N/m}^2,$$

$$d_{31} = 23\times10^{-12}\,\text{C/N}.$$

The experimental evaluation of the theoretical analysis was conducted in the Robotics and Automation Laboratory at Michigan State University. In the laboratory, a microrobotic system, as shown in Figure 8, was used for the calibration and experiment work. It consists of a three-DOF micromanipulator

Figure 7 Prototypes of (a) the 1D and (b) 2D sensors

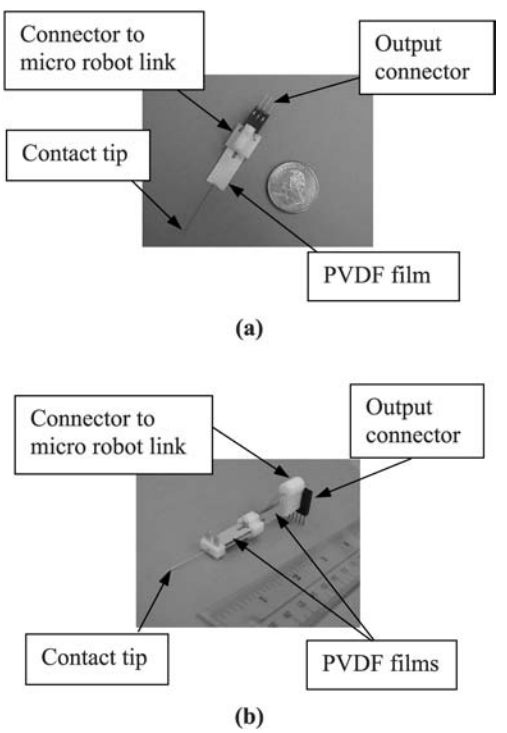

Figure 8 Microrobotic system at MSU

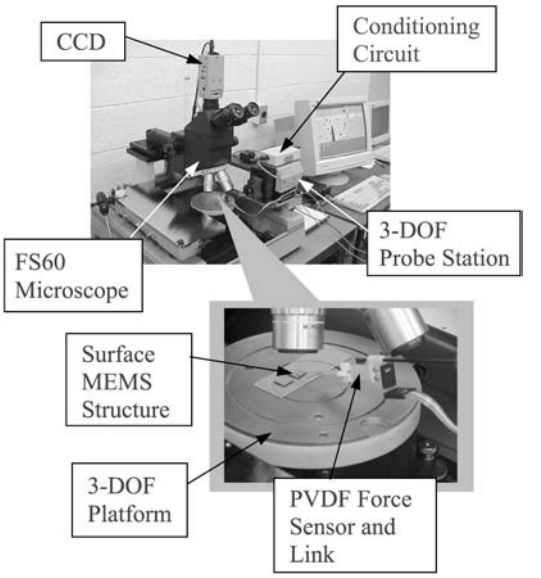

(SIGNATONE Computer Aided Probe Station), a three-DOF platform, a Mitutoyo FS60 optical microscope and a Sony SSC-DC50A CCD Color Video Camera. The microrobot is controlled by a PC-based control system. The robotic system is an open platform, which can easily be equipped with the PVDF force sensing system. Several motion control software and user interface have been developed. They provide a flexible and user-friendly platform to integrate with the force sensing system and control software.

When the PVDF sensor detects the microforce, the output voltage signals from the electronic circuit could be collected via a multifunction analog/digital input/output board (AX5411H) into a PC. Then there exists a force data communication between the PC and microrobotic system. The sampling frequency of the AX5411H is 1 kHz in the experiments. To reduce vibrations, an active vibration isolated table was used during the calibrations and experiments. Within the set-up, the proposed calibration method and experimental studies were conducted to test the performance of the developed force sensing system.

3.2 Calibration

By virtue of a precisely calibrated Mitutoyo 100× microscope (with a 50 × objective and a 2 × zoom), and a Sony CCD camera system, the set-up for calibration was built. The total resolution of the set-up approaches 0.2106μm/pixels in X and 0.2666μm/pixels in Y on the image plane, so the tiny bending angle $\theta(t)$ or deflection $\delta(t)$ of the sensor beam under the microscope can be measured when a microforce is exerted. Note that, to obtain an accurate $\theta(t)$ or

$\delta(t)$ from the captured image, image processing techniques and least-square method were adopted to find an optimal solution on $\theta(t)$ or $\delta(t)$. Meanwhile, based on the model equation, the output voltage signals transferred by the built circuit can be used to calculate the theoretical value of contact force. For example, Figure 9 shows test results when a non-magnetic, insulating and rigid block on three-DOF platform contacted the 1D force sensor. In this case, the calibrated final force is 4.5040×10^{-7} N; the theoretical final force is about 5.1205×10^{-7} N. The impact time is about 0.65 s. The small deviations between the theoretical final forces and the calibrated forces may be caused by the inverse piezoelectric affection and pyroelectric effects, which are not considered and fully compensated in the sensing model. The inaccurate electronic components and remaining few noises also play a role in producing the deviations. Calibration results in Figure 10 show the comparison curves between the calibration forces and theoretical forces. The curves are rather close, which clearly indicates the effectiveness of the sensor models. By calibration, the sensitivity of the 1D sensor was estimated to be 4.6602 V/μN, the 2D sensor was

Figure 9 Sensor calibration example: (a) output voltage; and (b) microcontact force

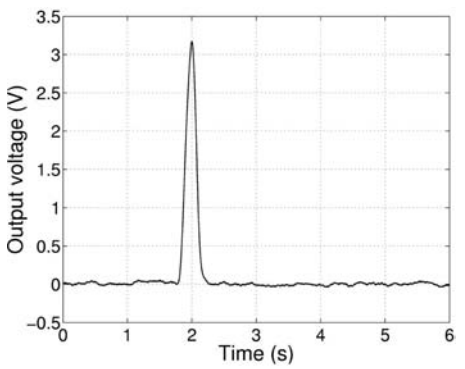

Figure 10 Comparison of theoretical and calibrated forces

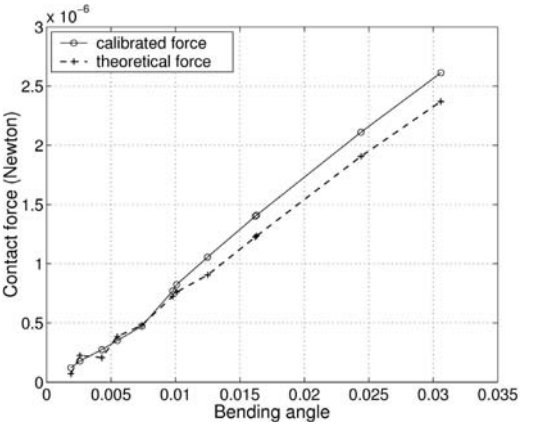

2.3985 V/μN (the gap distance of two films is zero). The resolutions of the sensors are both in the range of sub-micronewtons.

As an important aspect of the sensor, dynamic range is an ability to respond to signals having both large and small amplitude variation. The output width of sensor system is 12 V with a quantization resolution of 0.73 mV; therefore the output dynamic range of two sensors is 84.32 dB.

The input resolution of the sensor approaches 10^{-7} N. In analogy with output dynamic range, the input dynamic range is thus given by the ratio of input width to the input resolution. By calibration, when the sensor tip deflects to approach 90°, the input dynamic range of the 1D sensor is more than 104.4 dB; the 2D sensor is about 121.9 dB.

Furthermore, an experiment on the contact sensing was conducted. By using the 2D sensor, a continual contact-stop sensing experiment was implemented when the sensor tip acted on a planar glass surface that was set up in the *ZX* plane (referring to Figure 4). The 2D force signals recorded were plotted in Figure 11. The result

Figure 11 Response of 2D sensor when the force is exerting along *Y*

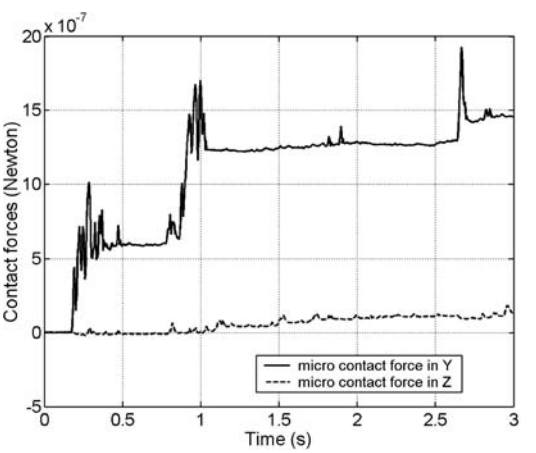

verified the performance of sensing and self-decoupling of the 2D force sensor.

4. Applications

4.1 Force-guided microassembly

With the use of the PVDF sensor, the force guided assembly technology of the surface MEMS structures was successfully developed, i.e. force guided assembly of micromirrors. In this application, a MUMPs micromirror chip, was used to test the developed force guided microassembly scheme. The 1D PVDF force sensor attaching a contact tip was mounted at the front end of the three-DOF micromanipulator. The assembly task includes multiple segments. Firstly, the tip was moved to the position under a micromirror. The tip, then, lifted the mirror up to an upright position until to be locked by the latches. At last, the tip went back to the initial position and will be ready for the next assembly of micromirror.

By virtue of the developed sensor-referenced force regulation scheme, as shown in Figure 12, the whole assembly process can be performed automatically. This controller characteristically utilizes the force, force rate, and positive acceleration feedbacks together with a switching control strategy to achieve a stable microcontact/impact force regulation in the assembly of micromirrors.

Figure 13 shows a successful assembly sequence of a MUMPs micromirror using the developed force-guided assembly scheme. Figure 14 gives a sketch of lifting up a micromirror by the sensor tip. Reference to Figure 14, during the lift-up assembly, the gravity force is not a dominative force in microenvironment, the forces exerted on the tip are mainly from the counteraction moments of the hinges and the latches, the friction forces due to the tip slides on the bottom surface of the mirror and the adhesion forces.

When the tip was moved along -Y to push slowly the micromirror up, the 1D sensor detects the microforce and its rate along Z, the force and its rate were then fed back to the force regulation controller in real time, as a result, the contact force can be regulated to approach a desired and safe force during the lifting up. By the analysis of action forces, to regulate the contact force along Z, the tip is adjusted automatically to slide up along the bottom surface of the micromirror, thus it promotes the lift-up of the micromirror until the micromirror is locked by the latches. Force and position data during the lift-up assembly were plotted in Figure 16 when the setting of the desired contact force is $F_c^d = 5.5 \times 10^{-6}$ N and the gains are $k_s = 1$, $k_f = 20$, $k_I = 20$. As shown in Figure 15(a), when the sensor tip approached to contact the micromirror, a downward with a spike in the force plot demonstrates an adhesive force that pulled the sensor tip toward the micromirror before the contact actually occurs. The tip positions were plotted in Figure 15(b).

Figure 12 Sensor referenced control scheme for microassembly

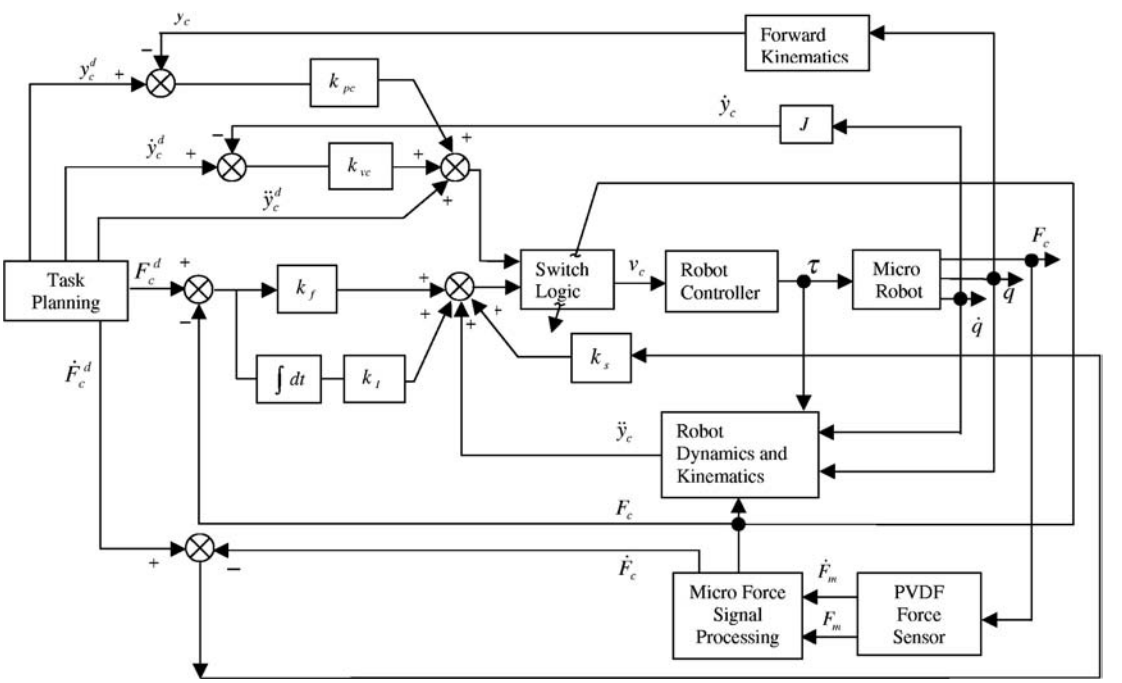

Figure 13 Micromirror force-guided assembly: (a) a sensor tip and a micromirror; and (b) the sequence of force-guided lift up micromirror

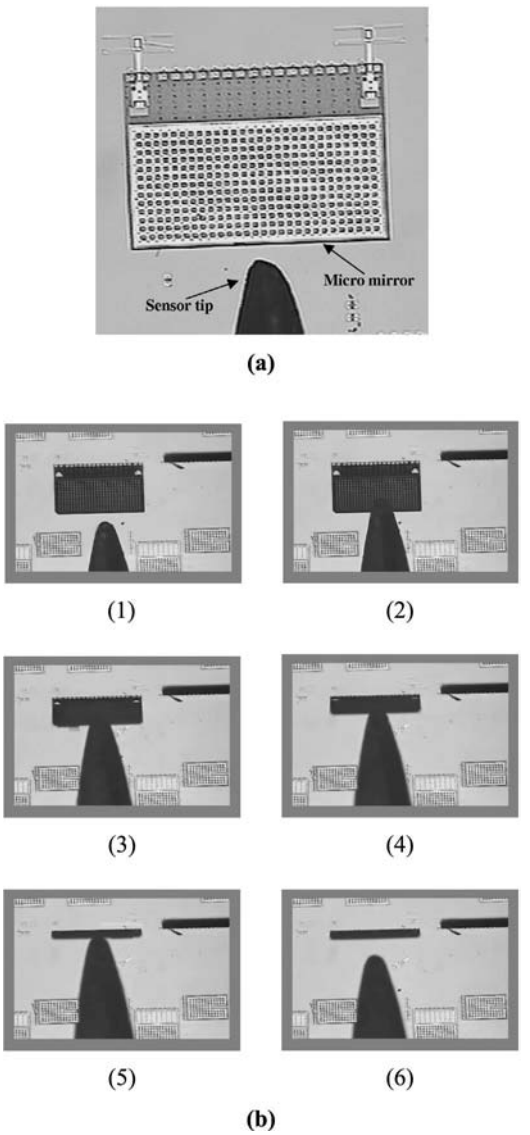

Experimental results clearly verified that micromirror assembly was realized reliably by the developed force-guided assembly scheme and the microcontact force can be regulated to keep a safety margin in the assembly.

4.2 Tele-micromanipulation with visual and haptic feedback

An "*e-MEMS*" concept is induced when we tele-assemble the MEMS structures via Internet. In this application, a master device with force/haptic feedback is driven to teleoperate a micromanipulator with the microforce sensor to assemble MEMS devices. Upon this concept, a micromanipulator-joystick tele-microassembly platform was built at Michigan State University, as shown in Figure 16. In this platform, we can

Figure 14 Sketch of lifting up a micromirror

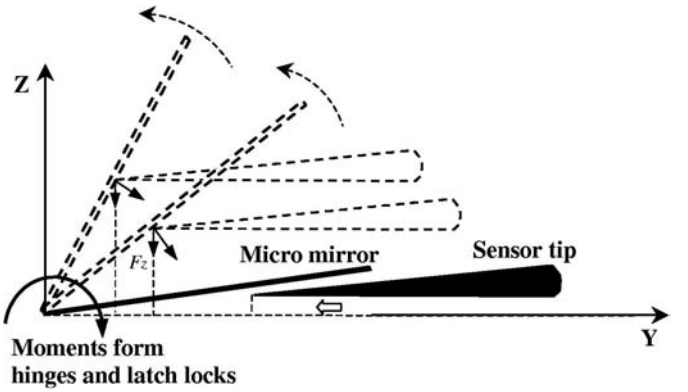

Figure 15 1D Force-guided assembly results: (a) contact force along *Z*; and (b) tip positions in *Y* and *Z*

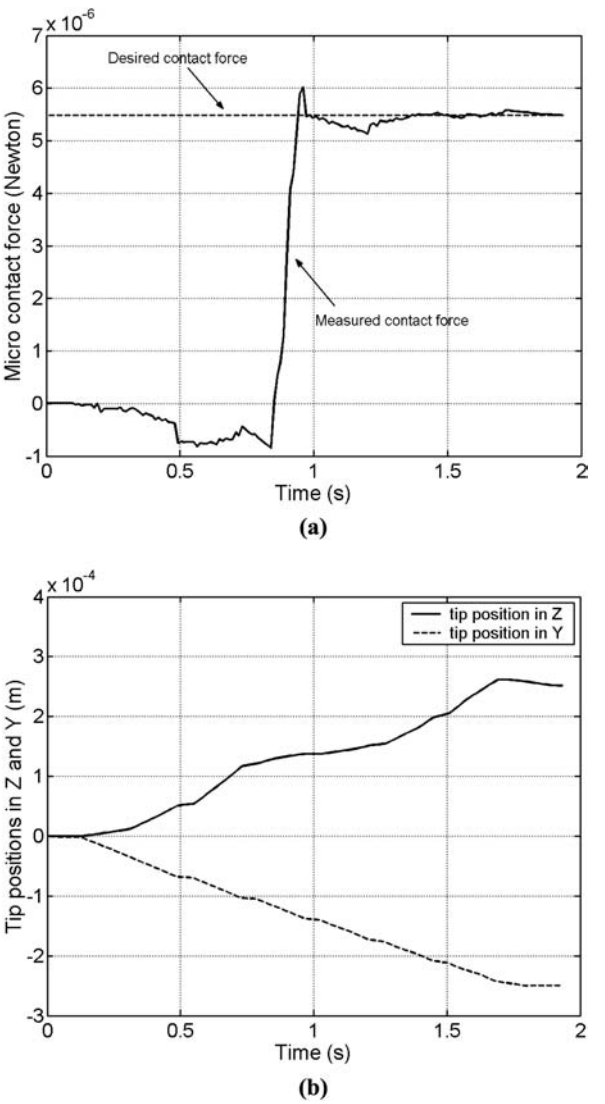

Figure 16 Tele-micromanipulatiion with visual/haptic feedback

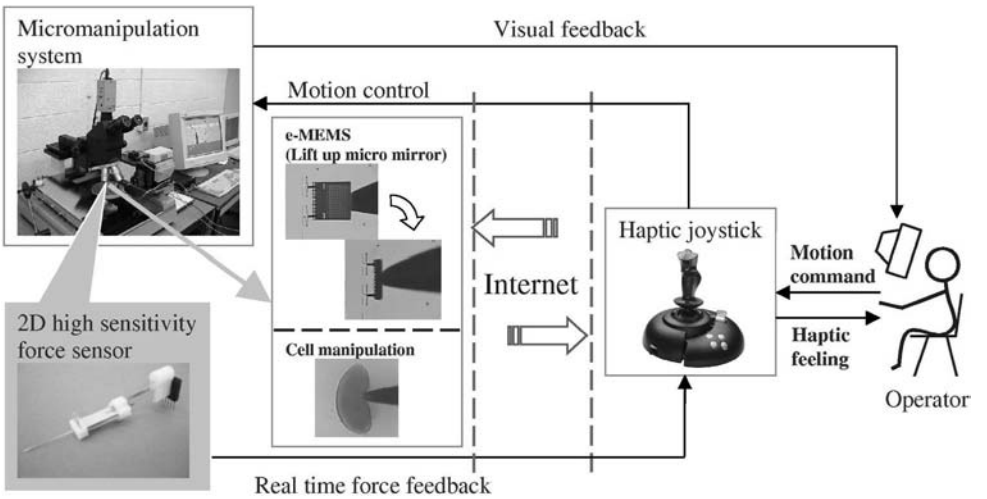

tele-assmeble the MEMS devices such as micromirrors with our hands. During the assembly, not only the visual feedback is provided for observing the situations of operation, but also the use of force feedback, which can provide the human operator with the similar haptic feeling even if the operator is not in direct assembling the micromirrors. The method used in this teleoperation is the motion-force transmission, in this case, the movement of the joystick is sent to the micromanipulator, and the microforces felt by the PVDF force sensor at the front end of micromanipulator are fed back to the joystick. By appropriately choosing the scaling laws, both the microforce and movement are effectively scaled up and down between the joystick and micromanipulator. The joystick used is a Microsoft SideWinder force feedback joystick.

The detailed procedure on the tele-microassembly of micromirror is as follows: before the lift-up, firstly, the operator drive the joystick to move the sensor tip to an initial position under the micromirror, then the tip is opearted to move forward and upward simultaneously, as a result, the moving tip begins to lift the micromirror up until the mirror approaching an upright position. With the assistance of visual feedback, and expecially force/haptic feedback, the task of tele-microassembly is achieved reliably and easily. Besides microassembly, recent advances in microbiology such as cloning demonstrate that increasingly complex micromanipulation strategies for manipulating biological cells are required. Our work meets this requirement greatly. By using the high sensitivity PVDF force sensor, as shown in Figure 16, the tele-cell-manipulation with force/haptic feedback via Internet can be realized using this micromanipulator-joystick platform. The cell used is the fruit fly embryo with the size of 400 μm × 100 μm. The technology can also be extended to advance cell manipulation or other complex bio-manipulations.

5. Conclusions

In this paper, we used PVDF film to fabricate high sensitivity 1D and 2D force/force rate sensors for assembly of microdevices such as surface MEMS structures fabricated using MUMPs process or biomanipulation. Based on the developed sensors, by using an electronic circuit designed with effective signal conditioning techniques, the microcontact force/impact signal can be extracted desirably so as to improve the reliability of microassembly/micromanipulation. Calibration and experimental results verified the performance of the sensors which demonstrate a high sensitivity and a resolution in the range of sub-micronewtons. The technology can provide the practical applications in microassembly and bio-manipulation, and it will be a critical and major step towards the development of automated micromanufacturing processes for batch assembly of MEMS devices as well as the advancement of complex bio-manipulations.

References

Arai, F., Nonoda, Y., Fukuda, T. and Ooda, T. (1996), "New force measurement and micro grasping method using laser raman spectrophotometer", *Proceedings of 1996 IEEE International Conference on Robotics and Automation*, pp. 2220-5.

Benech, P., Chamberod, E. and Monllor, C. (1996), "Acceleration measurement using PVDF", *IEEE Transactions on*

Ultrasonics, Ferroelectrics, and Frequency Control, Vol. 43 No. 5, pp. 838-43.

Böhringer, K.F., Fearing, R.S. and Goldberg, K.Y. (1999), "Microassembly", in Shimon, Nof (Ed.), *The Handbook of Industrial Robotics*, 2nd ed., Wiley, New York, NY, pp. 1045-66.

Carrozza, M., Eisinberg, A., Menciassi, A., Campolo, D., Micera, S. and Dario, P. (2000), "Towards a force-controlled microgripper for assembling biomedical microdevices", *J. Micromech. Microeng.*, Vol. 10, pp. 271-6.

Cohn, M.B., Böhringer, K.F., Novorolski, J.M., Singh, A., Keller, C.G., Goldberg, K.Y. and Howe, R.T. (1998), "Microassembly technologies for MEMS", *Proceedings of SPIE Conference on Micromachining and Microfabrication*, Invited paper/plenary session.

Fatikow, S., Seyfried, J., Fahlbusch, S.T., Buerkle, A. and Schmoeckel, F. (2000), "A flexible microrobot-based microassembly station", *Journal of Intelligent and Robotic Systems*, Vol. 27, pp. 135-69.

Fearing, R.S. (1995), "Survey of sticking effects for micro parts handling", *Proceedings of 1995 IEEE/RSJ International conference on Intelligent Robots and Systems*, pp. 212-7.

Fung, C.K.M., Elhajj, I., Li, W.J. and Xi, N. (2002), "A 2-D PVDF force sensing system for micro-manipulation and micro-assembly", *Proceedings of the 2002 IEEE International Conference on Robotics and Automation*, pp. 1489-94.

Kenny, T. (2001), "Nanometer-scale force sensing with MEMS devices", *IEEE Sensors Journal*, Vol. 1 No. 2, pp. 148-57.

Kimura, Y. and Yamagimachi, R. (1995), "Intracyto-plasmic sperm injection in the mouse", *Biology of Reproduction*, Vol. 52 No. 4, pp. 709-20.

Koelemijer, S.K., Benmayor, C.L., Uehlinger, J-M. and Jacot, J. (1999), "Cost effective micro-system assembly automation", *Proceedings of Emerging Technologies and Factory Automation*Vol. Vol. 1, pp. 359-66.

Lee, C., Itoh, T. and Suga, R. (1996), "Micromachined piezoelectric force sensors based on PZT thin films", *IEEE Transactions on Ultrasonics, Ferroelectrics, and Frequency Control*, Vol. 43 No. 4, pp. 553-9.

Measurement Specialties Inc. (1999), *Piezo Film Sensors Technical Manual*, *Internet Version*.

Nelson, B., Zhou, Y. and Vikramaditya, B. (1998), "Sensor-based micro-assembly of hybrid MEMS devices", *IEEE Control System Magazine*, Vol. 18, pp. 35-45.

Roh, Y., Varadan, V.V. and Varadan, V.K. (2002), "Characterization of all the elastic, dielectric, and piezoelectric constants of uniaxially oriented poled pvdf films", *IEEE Transactions on Ultrasonics, Ferroelectrics, and Frequency Control*, Vol. 49 No. 6, pp. 836-46.

Sun, Y. and Nelson, B.J. (2001), "Autonomous injection of biological cells using visual servoing", in Rus, D. and Singh, S. (Eds), *Experimental Robotics VII*, Springer, London, pp. 169-78.

Yamagata, Y. and Higuchi, T. (1995), "A micro-positioning device for precision automatic assembly using impact force of piezoelectric elements", *Proceedings of 1995 IEEE International Conference on Robotics and Automation*Vol. Vol. 3, pp. 666-71.

Zesch, W. and Fearing, R. (1998), "Alignment of microparts using force controlled pushing", *SPIE Conference on Microrobotics and Micro-manipulation*, 2-5 November 1998, Boston, MA.

Further reading

Damjanovic, D., Muralt, P. and Setter, N. (2001), "Ferroelectric sensors", *IEEE Sensors Journal*, Vol. 1 No. 3, pp. 191-206.

Gehring, G.A., Cooke, M.D., Gregory, I.S., Karl, W.J. and Watts, R. (2000), "Cantilever unified theory and optimization for sensors and actuators", *Smart Material Structure*, Vol. 9, pp. 918-31.

IEEE standard (1987), "An American national standard: IEEE standard on piezoelectricity", *ANS/IEEE Std*, pp. 176-1987.

Ikeda, T. (1990), *Fundamentals of Piezoelectricity*, Oxford University Press, Oxford.

Sato, H., Fukuda, T., Arai, F., Itoigawa, K. and Tsukahara, Y. (2000), "Parallel-beam sensor/actuator unit and its application to the gyroscope", *IEEE/ASME Transactions on Mechatronics*, Vol. 5 No. 3, pp. 266-72.

Tarn, T.J., Wu, Y.Y., Xi, N. and Isidori, A. (1996), "Force regulation and contact transition control", *IEEE Control Systems*, pp. 32-40.

Weinberg, M.S. (1996), "Working equations for piezoelectric actuators and sensors", *IEEE Journal of Microelectromechanical Systems*, Vol. 8 No. 4, pp. 529-33.